AJNR

CT Angiography and MR Angiography in the Evaluation of Carotid Cavernous Sinus Fistula Prior to Embolization: A Comparison of Techniques

Clayton Chi-Chang Chen, Patricia Chuen-Tsuei Chang, Cherng-Gueih Shy, Wen-Shien Chen and Hao-Chun Hung

CT Angiography and MR Angiography in the Evaluation of Carotid Cavernous Sinus Fistula Prior to Embolization: A Comparison of Techniques

Clayton Chi-Chang Chen, Patricia Chuen-Tsuei Chang, Cherng-Gueih Shy,
Wen-Shien Chen, and Hao-Chun Hung

BACKGROUND AND PURPOSE: This study compared CT angiography (CTA), MR angiography (MRA), and digital subtraction angiography (DSA) in elucidating the size and location of carotid cavernous sinus fistulas (CCFs) before embolization treatment.

METHODS: This was a retrospective study of 53 patients with angiographically confirmed CCF. All patients underwent pre- and postcontrast-enhanced CTA and DSA, and 50 patients also underwent MRA. Two neuroradiologists rated detectability of the fistula tract as "good," "moderate," or "poor" in source images obtained by using each procedure. The χ^2 test was used to compare the imaging modalities with respect to their ability to detect fistulas.

RESULTS: CTA did not differ significantly from DSA ($P = .155$), and both CTA ($P = .001$) and DSA ($P = .007$) performed significantly better than MRA in the population as a whole. Differences in performance among the methods, however, depended upon the segmental location of the fistula along the internal carotid artery (ICA). CTA and MRA were similar in detection of CCFs in patients with a fistula at segment 3. CTA significantly outperformed MRA in patients with a fistula at segment 4, who accounted for approximately half of the population.

CONCLUSIONS: CTA source imaging has proved itself as useful as DSA for detecting CCFs. Of the 2 noninvasive techniques, CTA performed better than MRA in the population as a whole and in most patients whose fistula was located at segment 4 or 5 of the ICA.

Digital subtraction angiography (DSA) is commonly regarded as the best method of evaluating carotid cavernous fistulas (CCFs) before treatment by using an embolization procedure (1). DSA, however, has the disadvantage of being an invasive procedure. Furthermore, DSA sometimes fails to reveal the precise size and location of the fistula. Transcranial Doppler ultrasonography has been advocated as a noninvasive alternative to DSA in the diagnosis of CCFs (2, 3). Although Doppler ultrasonography is excellent in di-

agnosing both high-flow and low-flow fistulas, it does not provide precise details regarding their size and location. Alternatively, source images of CT angiography (CTA) and 3D time-of-flight (TOF) MR angiography (MRA) have been shown to provide more information about the size and location of fistulas (4–9). The purpose of this study was to assess the value of CTA and MRA source images, performed before embolization, in evaluating the size and location of fistula shunts and in elucidating venous drainage characteristics in CCFs by 3D reconstructed images.

Methods

Patients

This retrospective study enrolled 53 patients, 32 men and 21 women, ranging in age from 16 to 65 years, with angiographically confirmed CCF. These patients were treated at the neurosurgical, neurologic, or ophthalmic outpatient department clinics of Taichung Veterans General Hospital between January 1999 and December 2003. All patients provided informed consent for imaging and embolization procedures.

All 53 patients were screened by using both CTA and DSA before treatment. Fifty of the patients were also screened by using MRA. A total of 54 fistula tracts were detected in 53

patients (one patient had 2 fistula tracts). The interval between the traumatic episode and the imaging diagnosis ranged from 1 week to 14 years.

A total of 52 embolization procedures by using a detachable balloon or a Guglielmi detachable coil (GDC) were performed on 51 patients, with one patient being treated a second time because of fistula recurrence. Two of the patients were not treated, because they had spontaneous occlusion of the fistula induced by manual compression of the ipsilateral common carotid artery (CCA). These 2 patients had smaller fistulas.

Imaging Methods

All CT examinations were performed on spiral CT scanners (Picker PQ2000, PQ5000, and PQ6000; Picker International, Highland Heights, OH). Noncontrast-enhanced and contrast-enhanced CT scans of the brain were obtained in the axial section with a section thickness of 4 mm and without an intersection gap. The scanning parameters for CTA were as follows: collimation, 1 mm; pitch, 0.5; and index, 1 mm. The scan time, matrix, and field of view were 1 s/revolution, 512 × 512, and 20 × 20 cm, respectively. We scanned between the C2 vertebra and a level approximately 8 cm higher to cover the circle of Willis. The contrast-enhanced CT study was performed following insertion of a 20-gauge sheath needle into the anterior cubital vein. Approximately 95 mL of contrast media were injected at a flow rate of 3 mL/s by using a power injector. A delay time of 12 seconds was used to allow the contrast medium to reach the intracranial arteries before scanning. The contrast media were Telibrix (Guerbert, Roissy, France), Omipaque (Nycomed, Brussels, Belgium), or Ultravist (Schering, Berlin, Germany).

MR imaging was performed by using GE 1.5T Signa (Milwaukee, WI) or Siemens 1.5T (Erlangen, Germany) Sonata MR scanners. First, routine T1-weighted (500–600/12–20/1 [TR/TE/excitations]) and T2-weighted (3500–4000/80–90/1) spin-echo images and postgadolinium images were obtained in the axial and/or coronal plane through the orbital and sellar regions by using a section thickness of 5–6 mm. 3D TOF MRA was then performed by using the following parameters: 36/minimal/1; 25° flip angle; 32–40-mm slab thickness; 32 partitions; 24-cm field of view; and 512 × 256 matrix. The actual thickness of the partitions was 1.2 mm. The cavernous sinus was located at the center of the volume slab. The contrast medium was Magnevist (Schering, Berlin, Germany) or Dotarem (Guerbet, Roissy, France).

Selective cerebral DSA with anteroposterior and lateral projection was performed by using a Siemens Neurostar (Forchheim, Germany) biplane angiogram system. Through the femoral artery approach, selective injections of contrast medium (5–16 mL) in bilateral CCA and vertebral angiogram (VA) were given. Once a fistula was found, the angiograms of contralateral carotid or vertebral arteries injected with ipsilateral carotid compression were done, which resulted in retrograde filling of the fistula via the ipsilateral posterior communicating artery and the cavernous carotid segment (Huber maneuver).

Interpretation of Images

Contrast-enhanced CT scans and spin-echo MR images were reviewed to establish the diagnosis of CCF as well as to find any associated vascular abnormalities. Individual source images of CT and MR angiograms rather than integrated images from each scanning method were used to identify the size and location of the fistula tract and the venous drainage. Two neuroradiologists (C.C.C.C. and C.G.S.) independently analyzed each image for the following findings:

● Size and location of the fistula tract —The location of the fistula tract was described by the segmental division of the ICA according to the classification of Debrun et al (10) (Fig 1):
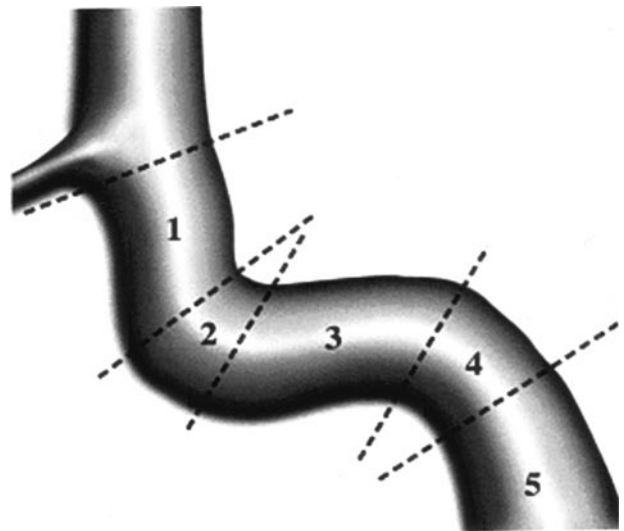

Fig 1. Segmental division of the cavernous carotid artery (after Debrun et al [10]).

● Cavernous sinus morphology—This was categorized into 3 forms: pseudoaneurysmal (bulging), sinusoidal (less bulging), or channel-like (channel formation between the artery and the eye)
● Presence or absence of dilation of the ophthalmic vein (OV; right or left superior or inferior) or facial vein
● Pattern of venous sinus drainage—right or left superior petrous, inferior petrous, or sphenoparietal sinus
● Presence or absence of engorged pial-cortical veins and/or deep vein drainage
● Presence or absence of venous aneurysm and/or venous sinus varix
● Presence or absence of cervical artery dissection on the ipsilateral or contralateral side to the affected carotid artery.

The wall of the ICA was generally well defined in both CTA and MRA images; in these instances, the fistula ostium was located by following the wall of the ICA until its boundary became indistinct, showing the presence and width of the connection between the ICA and the cavernous sinus.

For each imaging technique, the neuroradiologists rated the detectability of the fistula tract as "poor" (neither the size nor the location of fistula could be defined), "moderate" (either the size or the location of fistula could be defined), or "good" (both the size and location could be defined).

A diagnosis of CCF was made by CT if focal bulging or diffuse distension of the cavernous sinus and/or enlargement of the superior OV (SOV) were found (11, 12). In the case of spin-echo MR images, CCF was diagnosed if the above criteria for CT were met and also flow void was observed within the cavernous sinus.

Each patient's CTA and MRA images were evaluated before performing the DSA study, which was considered to represent the "gold standard." The 2 radiologists reached a consensus regarding the detectability of each fistula and recorded their joint assessment. If possible, they based their plan for treatment (generally embolization) on the CTA and MRA results. They then obtained a DSA study to confirm the location of the fistula and performed the embolization as soon as the DSA results were available for correlation with the CT and MR images.

Embolization was carried out by using a detachable balloon or a coil to occlude the fistula ostium or the parent artery. Spontaneous occlusion of the fistula occasionally occurred as a

Comparison of imaging modalities for their ability to detect carotid cavernous fistula tracts

Modality (Fistula Tracts Identified)	Ability to Detect Fistula Tracts, n (%)*			P Value (Chi-square Test)			
	Poor	Moderate	Well	Overall	CTA vs DSA	CTA vs MRA	MRA vs DSA
CTA ($n = 54$)	7 (13.0)	13 (24.1)	34 (63.0)				
MRA ($n = 50$)	10 (20.0)	26 (52.0)	14 (28.0)	.002	NS	.001	.007
DSA ($n = 54$)	3 (5.6)	21 (38.9)	30 (55.6)				

Note.—CTA indicated computed tomography angiography; MRA, magnetic resonance angiography; DSA, digital subtraction angiography; NS, not significant.

* Poor indicates neither size nor location of fistula can be defined; moderate, either size or location of fistula can be defined; well, both size and location of fistula can be defined.

result of ipsilateral carotid compression. The exact location of the fistula tract was finally verified by using the results of DSA imaging and/or confirming its location during the embolization procedure.

Data Analysis

Statistical analysis of the fistula detectability scores from the CTA, MRA, and DSA images was performed by using SPSS software, version 11.5 (SPSS Inc., Chicago, IL). The χ^2 test was used to assess whether the 3 imaging modalities differed with respect to the proportion of fistulas rated as good, moderate, or poor for the entire population. The patients were then grouped according the segmental location of their fistulas, and the imaging methods were compared statistically within each group. Three pairwise comparisons between imaging modalities were also made for the patient population as a whole and within each group defined by fistula location. To adjust for multiple comparisons, statistical significance was concluded only if a P value was ≤.0167 (.05/3).

Results

Fifty-four fistula tracts were identified, one tract in each of 52 patients and 2 tracts in one patient. In most of the 53 patients, the fistula was located at either ICA segment 4 (29 patients [55%]) or segment 3 (19 patients [36%]). The remaining patients (6/53 [11%]) had a fistula at ICA segment 5. No patient was found to have a fistula at segment 1 or 2.

The Table presents the fistula detectability ratings for the patient population as a whole. The distribution of ratings differed significantly among the 3 methods ($P = .002$). Pairwise comparisons indicated that MRA was less reliable in detecting the size and location of fistula tracts than either CTA ($P = .001$) or DSA ($P = .007$). Nevertheless, MRA proved to be a reasonably useful method, because fistula detectability was rated as moderate or good in most of the patients (40/50 [80%]) who had an MRA evaluation.

In Fig 2, detectability ratings are compared according to the segmental location of the fistula for each imaging technique. As shown in Fig 2*A,* CTA performed significantly better in identifying fistulas located at segmental division 4 compared with those at division 3. The performance of DSA and MRA did not depend on the location of the fistula (Fig 2*B, -C*).

It was notable that the differences in performance among the 3 imaging methods were dependent upon the location of the fistula along the ICA (Fig 3). For 19 patients with a fistula located in segment 3, neither the overall difference among methods nor any pairwise difference between methods was found to be statistically significant (Fig 3*A*). CTA and MRA images were very similar in their ability to detect fistulas located at segmental division 3.

Approximately half of the patients had a fistula located in segmental division 4. Within this group of 29 patients, the neuroradiologist rated the detectability of fistulas by using CTA as moderate or good in all patients except one. The results from CTA imaging were statistically similar to those from DSA angiograms ($P = .348$; Fig 3*B*). CTA ($P < .001$) provided significantly better performance than MRA for fistulas located at segment 4 (Fig 3*B*).

The results in the group of 6 patients with a fistula located at segment 5 appeared to be qualitatively similar to the larger group with fistulas at segment 4. The differences between imaging methods were not statistically significant, probably due to the small number of patients within this group (Fig 3*C*).

Figure 4 shows individual imaging results from a 21-year-old female motorcycle-crash victim, who presented with left-eye proptosis and intracranial bruit of 2 weeks' duration. The fistula tract between the ICA and the cavernous sinus at segment 3 could be visualized by using CTA (panels *A–C*) and MRA (panels *D–F*). The results from both CTA and MRA correlated well with the flow of contrast material observed in a VA (lateral views in panels *H* and *I*). Fistula detectability was rated as good for both the CTA and the DSA images and moderate for MRA.

Figure 5 shows source images made by using CTA (panels *A–C*) and MRA (panels *D–F*) in a 32-year-old man who presented with proptosis of the right eye. This patient had been injured in a motorcycle crash 3 weeks earlier. Both CTA and MRA indicated the presence of a fistula at segment 3 of the right ICA. A connection was suspected between the ICA and the OV, because the portion of the ICA distal to the fistula ostium could not be visualized. Transection of the ICA was later confirmed by results from MIP reconstruction MRA (panel *G*) and carotid DSA (lateral view in panel *H*). The decision to use a detachable balloon to occlude the ICA proximally was based on the features seen in both CTA and MRA images. The neuroradiologists assessed fistula detectability as good for both modalities, as well as DSA.
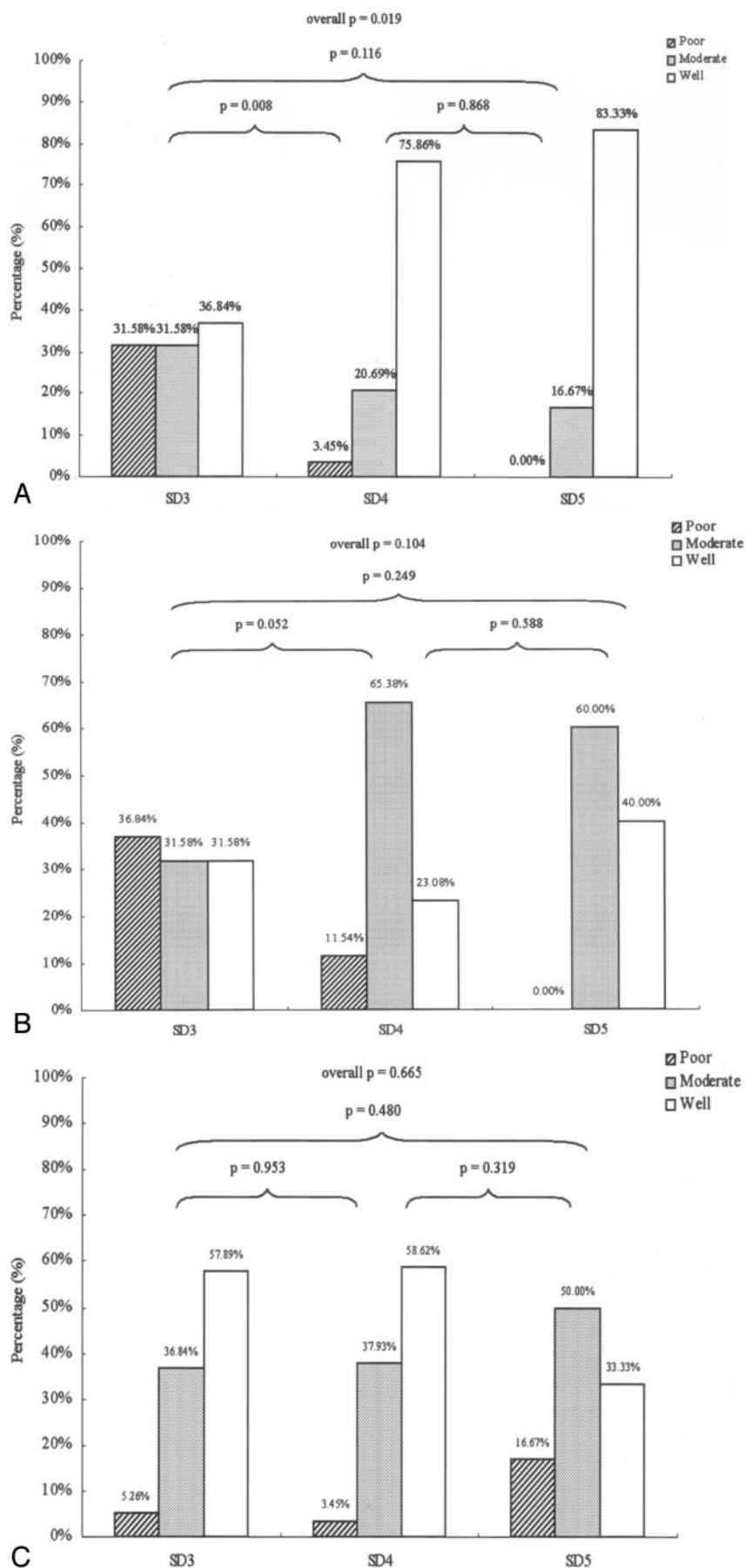
FIG 2. Detectability of CCFs by location according to segmental division (SD) of the ICA, by using each technique. Panels *A, B,* and *C* show results for CTA, MRA, and DSA, respectively. Bars indicate percentage of images having detectability ratings of poor (hatched), moderate (stippled), or good (open). *P* values indicate statistical significance for comparisons between locations by using the χ^2 test, for each technique.

Fig 3. Detectability of CCFs by using CTA, MRA, and DSA, by location according to segmental division (SD) of the ICA. Panels *A, B,* and *C* show results for fistulas found at SD 3, SD 4, and SD 5, respectively. Bars indicate percentage of images having detectability ratings of poor (hatched), moderate (stippled) or good (open). *P* values indicate statistical significance for comparisons between modalities by using the χ^2 test, for each location.
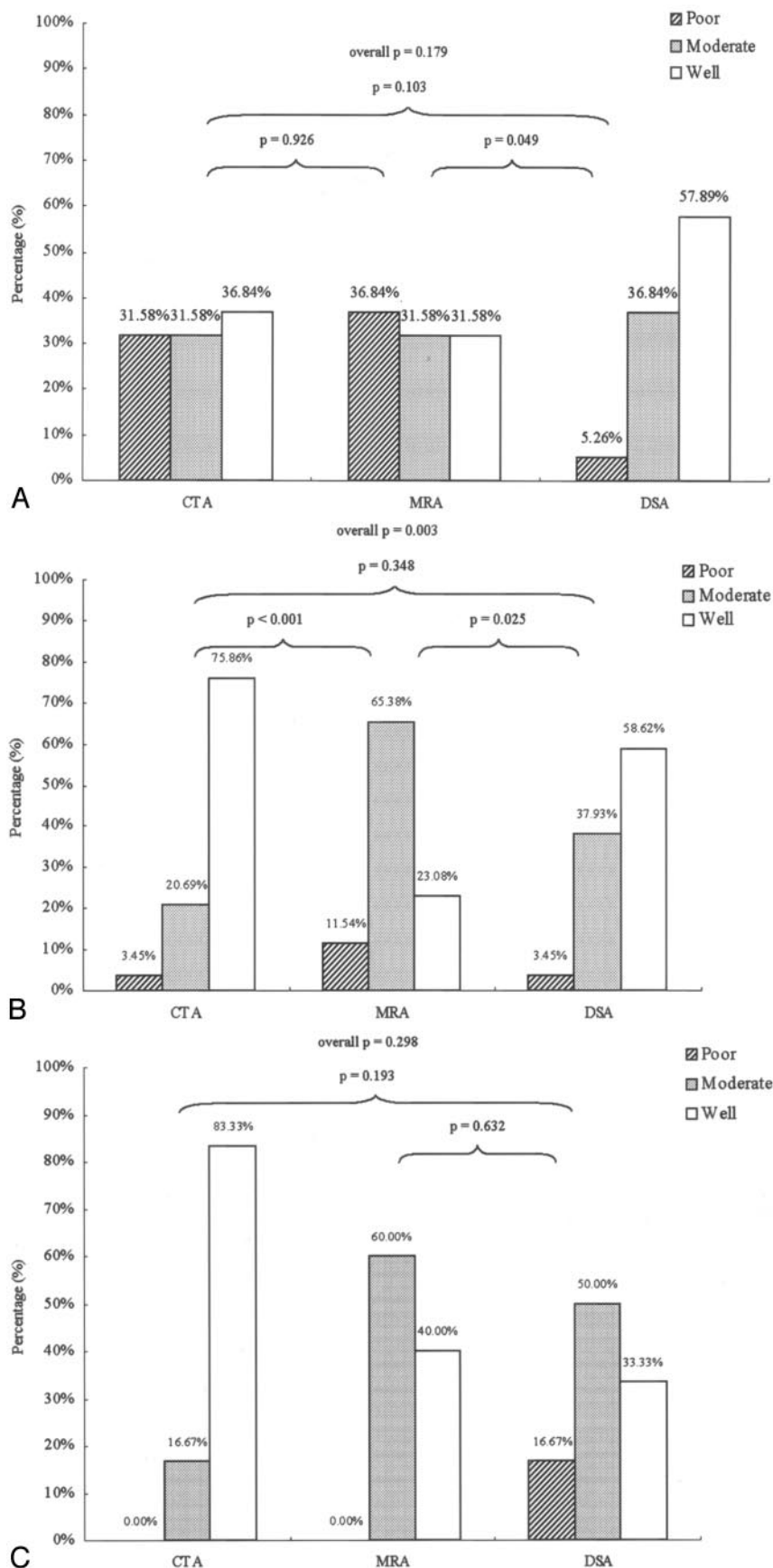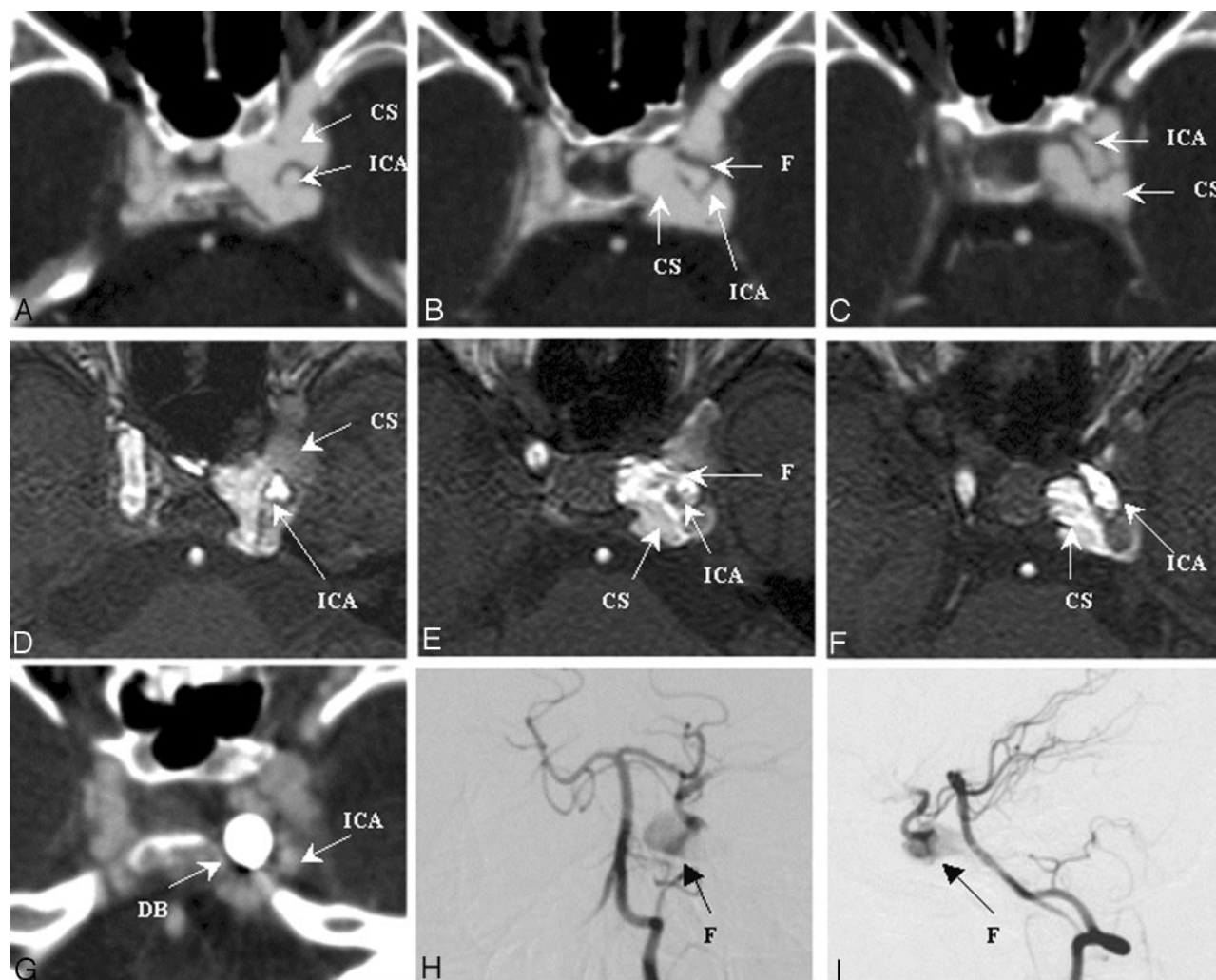
FIG 4.   SD 3, DSA = CTA > MRA. Left CCF with left SOV drainage.
Images were made by using CTA (panels A–C), MRA (panels D–F), and vertebral DSA (posterior-anterior view in panel H, lateral view in panel I) before embolization. The fistula ostium (panels B and E), proximal portion (panels A and D), and distal portion (panels C and F) are shown. A CTA source image made following embolization (panel G) shows the detachable balloon located at the previous fistula site. CS, cavernous sinus; DB, detachable balloon; F, fistula tract; SD, segmental division of the ICA.

Discussion

The diagnosis of traumatic CCF is made primarily from the findings of conventional angiography. Traumatic CCFs, however, are all direct high-flow shunts of Barrow et al type A (13). Because rapid flow can fill the CS and obscure the fistula site, a conventional carotid DSA study may not adequately visualize the fistula tract. Injecting contrast medium into the ipsilateral intracavernous carotid artery (Mehringer-Hieshima maneuver) or vertebral artery (Huber maneuver) while compressing the carotid artery on the lesion side can obviate this difficulty to some extent. Nonetheless, a rare double fistula was missed in a DSA study for one of our patients.

Recent developments in noninvasive techniques such as CTA and MRA have provided useful new tools for the early and safe diagnosis of these vascular disorders before treatment. Previous reports have shown that contrast-enhanced CT and MR imaging are helpful in the assessment of CCFs (4–9). Mor-

phologic changes such as dilation of the SOV, cavernous sinus, and protrusion of the globe have been well demonstrated by contrast-enhanced CT and MR imaging. CT and MR angiograms are also able to depict abnormal vascular changes, including engorged venous sinuses or cortical vein drainage, arterial or venous aneurysm formation, and arterial dissection.

In our study, source images of CTA and 3D TOF MRA proved useful in identifying fistulas before an invasive DSA study was undertaken. CTA and/or MRA source images provided essential information that was not obtainable by using DSA in some cases. The patient illustrated in Fig 4 was found by CTA and MRA to have a tiny fistula tract. With the conventional procedure, the detachable balloon occasionally cannot pass into the CS through a narrow fistula. On the basis of the CTA/MRA results in this patient, we chose a different method of embolization, the double-balloon pushing technique (14). We were able to successfully treat this fistula while saving the ICA.
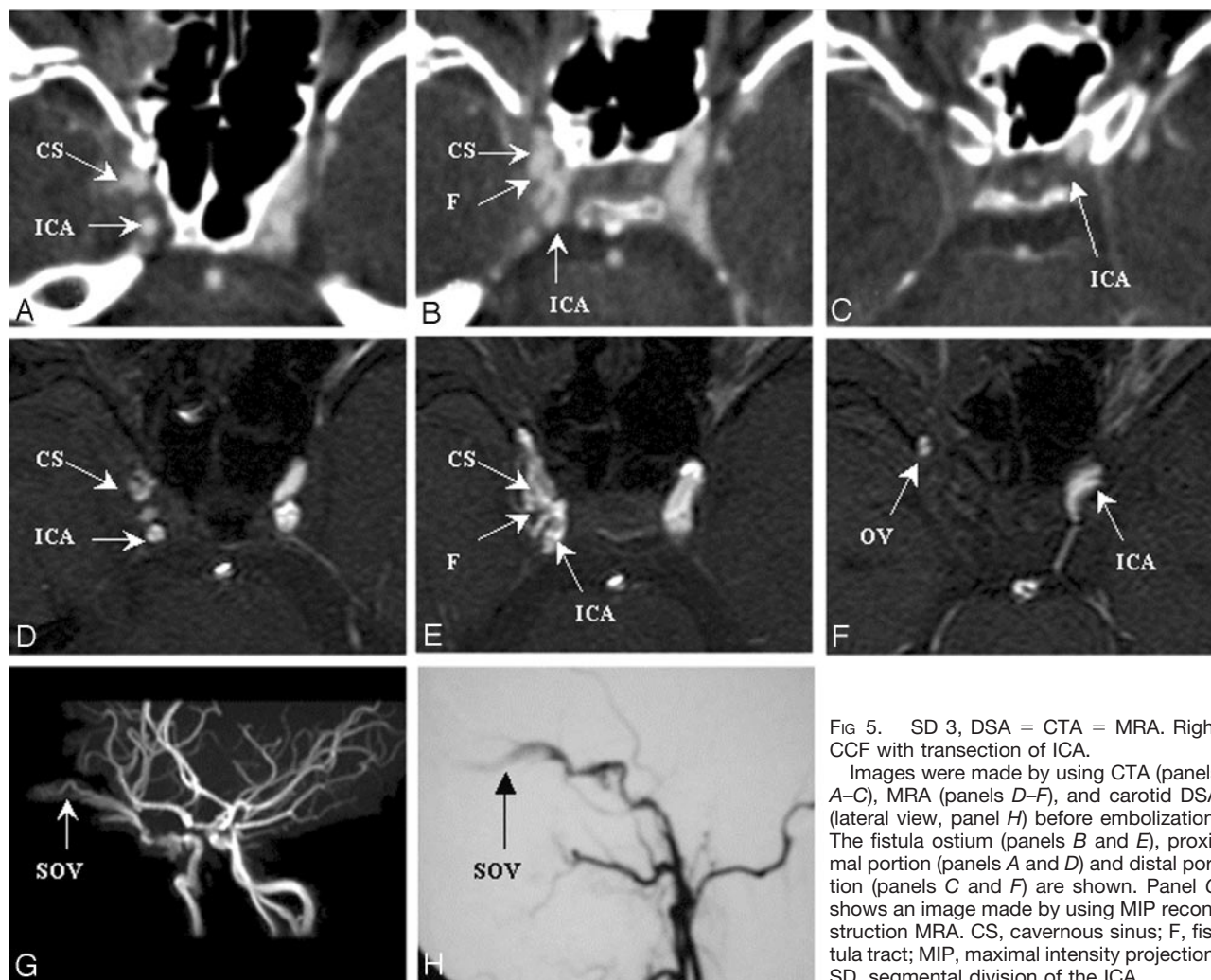
Fig 5. SD 3, DSA = CTA = MRA. Right CCF with transection of ICA.

Images were made by using CTA (panels A–C), MRA (panels D–F), and carotid DSA (lateral view, panel H) before embolization. The fistula ostium (panels B and E), proximal portion (panels A and D) and distal portion (panels C and F) are shown. Panel G shows an image made by using MIP reconstruction MRA. CS, cavernous sinus; F, fistula tract; MIP, maximal intensity projection; SD, segmental division of the ICA.

As another example, the patient in Fig 5 had a large fistula connecting the right ICA and the OV, with dissection and complete occlusion of the ICA distally. The fistula was well visualized by using either CTA or MRA. Having this information before intervention allowed us to recognize that effective treatment would require sacrifice of the parent artery.

The use of gadolinium-enhanced 3D TOF MRA or contrast-enhanced MRA has been reported in the follow-up of intracranial aneurysms treated with detachable coils (15, 16). The high resolution and sensitivity to flow of these techniques were useful in identifying residual patency and extent of recanalization for large aneurysms (15). It was noted, however, that contrast-enhanced conventional sequences did not seem to be indicated for small aneurysms or for those located near the base of the skull, where enhancement of veins could interfere with the evaluation of adjacent arteries (15).

We performed contrast-enhanced MRA in 42 of our CCF patients. Our experience was that the cost of a shortened acquisition time with a lower matrix (128 × 256) was a decrease in spatial resolution that made evaluation of the fistula tract difficult. Similarly, Hirai et al concluded that contrast-enhanced 3D TOF MRA was effective in delineating venous structures and distal arteries but not the flow dynamics within the cavernous sinuses, which were homogeneously enhanced (5).

We considered the possibility of bias in detectability scores, because the images were evaluated in an unblinded manner by observers who knew the patients' symptoms and any previous imaging results. A blinded reading was not possible because these 2 readers were the only persons at our institutions with the necessary clinical expertise. There are 2 reasons that any bias in detectability scores would favor DSA over CTA and MRA. First, CTA and MRA results were always obtained before DSA. Any clues from the former might improve detectability ratings for the latter. Second, the learning curve for reading CTA and MRA images was most prominent for the first patients of the series and might reduce detectability ratings for those modalities. Before this article was written, all cases were reviewed and the detectability ratings were reassessed and corrected if necessary.

The performance of CTA was better than or similar to that of MRA in detecting the location of fistulas in most of our patients. The size of the communicating tract between the ICA and the adjacent cavernous

sinus could be estimated quite often by using source images from CTA but relatively infrequently by using source images from 3D TOF MRA, because flow-related artifacts resulted in difficulties in identifying the size of the fistula tract.

The differences between the modalities in detecting CCFs, however, were dependent on the location of the fistula. Approximately one-third of the patients had a fistula located in segmental division 3. For these patients, CTA and MRA were similar in their ability to detect CCFs, and both were somewhat less effective than DSA (difference not statistically significant; Fig 3*A*). One possible explanation is that the plane of the fistula is parallel to the plane of the section in source images from both CTA and MRA, if the fistula is located at segment 3.

Approximately half of our patients had a fistula located at segmental division 4. Within this group, CTA source images identified the fistula tract as good in 76% (22/29) of the patients and performed significantly better than MRA source images (Fig 3*B*).

Conclusion

CTA source imaging has proved itself as useful as DSA for detecting CCFs. Of the 2 noninvasive techniques, CTA performed better than MRA in the population as a whole and in most patients, whose fistula was located at segment 4 or 5 of the ICAs.

References

1. Modic MT, Berlin AJ, Weinstein MA. **The use of digital subtraction angiography in the evaluation of carotid cavernous sinus fistulas.** *Ophthalmology* 1982;89:441–444
2. Killic T, Elmaci I, Bayri Y, et al. **Value of transcranial Doppler ultrasonography in the diagnosis and follow-up of carotid-cavernous fistulae.** *Acta Neurochir (Wien)* 2001;143:1257–1264
3. Molnar LJ, Caldas JG, Garcia RG, Cerri GG. **Doppler mapping of direct carotid-cavernous fistulae (DCCF).** *Ultrasound Med Biol* 2001;27:367–371
4. Coskun O, Hamon M, Catroux G, et al. **Carotid-cavernous fistula: diagnosis with spiral CT angiography.** *AJNR Am J Neuroradiol* 2000;21:712–716
5. Hirai T, Korogi Y, Hamatake S, et al. **Three-dimensional FISP imaging in the evaluation of carotid cavernous fistula: comparison with contrast-enhanced CT and spin-echo MR.** *AJNR Am J Neuroradiol* 1998;19:253–259
6. Ohtsuka K, Hashimoto M. **The results of serial dynamic enhanced computed tomography in patients with carotid-cavernous sinus fistulas.** *Jpn J Ophthalmol* 1999;43:559–564
7. Ouanounou S, Tomsick TA, Heitsman C, et al. **Cavernous sinus and inferior petrosal sinus flow signal on three-dimensional time-of-flight MR angiography.** *AJNR Am J Neuroradiol* 1999;20:1476–1481
8. Cares HL, Roberson GH, Grand W, Hopkins LN. **A safe technique for the precise localization of carotid cavernous fistula during balloon obliteration: technical note.** *J Neurosurg* 1978;49:146–149
9. Chen J, Tsuruda JS, Halbach VV. **Suspected dural arteriovenous fistula: results with screening MR angiography in seven patients.** *Radiology* 1992;183:265–271
10. Debrun G, Lacour P, Vinuela F, et al. **Treatment of 54 traumatic carotid-cavernous fistulas.** *J Neurosurg* 1981;55:678–692
11. Ahmadi J, Teal JS, Segall HD, et al. **Computed tomography of carotid-cavernous fistula.** *AJNR Am J Neuroradiol* 1983;4:131–136
12. Uchino A, Hasuo K, Matsumoto S, Masuda K. **MRI of dural carotid-cavernous fistulas: comparisons with postcontrast CT.** *Clin Imaging* 1992;16:263–268
13. Barrow DL, Spector RH, Braun IF, et al. **Classification and treatment of spontaneous carotid-cavernous sinus fistulas.** *J Neurosurg* 1985;62:248–256
14. Teng MMH, Chang CY, Chiang JH, et al. **Double-balloon technique for embolization of carotid cavernous fistulas.** *AJNR Am J Neuroradiol* 2000;21:1753–1756
15. Anzalone N, Righi C, Simionato F, et al. **Three-dimensional time-of-flight MR angiography in the evaluation of intracranial aneurysms treated with Guglielmi detachable coils.** *AJNR Am J Neuroradiol* 2000;21:746–752
16. Leclerc X, Navez JF, Gauvrit JY, et al. **Aneurysms of the anterior communicating artery treated with Guglielmi detachable coils: follow-up with contrast-enhanced MR angiography.** *AJNR Am J Neuroradiol* 2002;23:1121–1127